Journal of Atmospheric and Solar–Terrestrial Physics 278 (2026) 106698

Contents lists available at ScienceDirect

Journal of Atmospheric and Solar-Terrestrial Physics

journal homepage: www.elsevier.com/locate/jastp

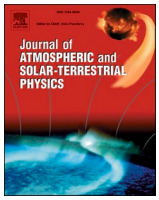

Research Paper

The impact of $PM_{2.5}$ sources on the single scattering albedo at a rural site in the south-western Mediterranean region

J.F. Nicolás *, J. Crespo, E. Yubero, M. Alfosea-Simón, A. Clemente, N. Gómez-Sanchez, N. Galindo

Atmospheric Pollution Laboratory (LCA), Department of Applied Physics, Miguel Hernández University, Avenida de la Universidad S/N, 03202, Elche, Spain

ARTICLE INFO

Keywords:
Aerosol sources
Rural site
MLR
Single scattering albedo
Scattering
Absorption

ABSTRACT

In the present work, the contribution of $PM_{2.5}$ sources to light absorption ($\sigma_{ap,520}$) and scattering ($\sigma_{sp,525}$), as well as their impact on SSA values, was analysed. For this, measurements of aerosol optical properties and $PM_{2.5}$ chemical composition were conducted at a rural site in southeastern Spain. The sources that significantly contributed to light extinction were: road traffic (TR), biomass burning (BB), mineral dust (MD), and a secondary aerosol source (SA). BB accounted for nearly 50 % of the absorption coefficient ($\lambda = 520$ nm), while the SA source exhibited the largest contribution to the scattering process (~47 % at 525 nm). MD showed the smallest contribution to $\sigma_{ap,520}$ and $\sigma_{sp,525}$, although its contribution significantly increased during Saharan dust events (SDEs). SSA daily values showed a clear dependence on the contribution of individual sources to $PM_{2.5}$ concentrations. SSA values ($\lambda = 525$ nm) exceeding 0.90 were observed when contributions from secondary aerosols were greater than 50 %, while the SSA decreased with the increase in the contribution from road traffic. The contribution from BB was fairly constant for almost all SSA values, although high SSA values (>0.90) were observed when the contribution from this source was very low. The SSA showed a clear spectral dependence that varied according to the aerosol type. So, for BB aerosols the SSA decreased with wavelength, while for mineral dust the opposite trend was observed.

1. Introduction

Atmospheric aerosols are a complex mixture of organic and inorganic compounds varying in size and optical properties, which depend on emission sources and atmospheric processes. Aerosols can have harmful effects on human health (Lelieveld et al., 2019), contribute to the corrosion and soiling of materials (Tzanis et al., 2011) and degrade air quality (Varotsos et al., 2012; Pérez-Vizcaíno et al., 2026). Moreover, they can affect climate. In this regard, aerosol optical properties critically influence the magnitude and sign of direct aerosol radiative forcing on a regional basis (Pani et al., 2023). Most aerosol components (mainly sulfate, nitrate, organic matter, soil dust and sea salt particles) scatter the sunlight (Pandolfi et al., 2018; Li et al., 2022). In contrast, other types of aerosols, such as black carbon (BC), brown carbon (BrC) and mineral dust (MD) absorb solar radiation (Moosmüller et al., 2009). The main sources of aerosol chemical components contributing to light extinction (the sum of absorption and scattering) are traffic exhaust, biomass burning (BB), secondary aerosol formation and mineral dust emissions.

The light absorption and scattering capacity for each source or chemical species can be evaluated by means of its Mass Absorption Efficiency (MAE) and Mass Scattering Efficiency (MSE). Both are key optical parameters for the evaluation of the light absorption and scattering ability of aerosols (Bond and Bergstrom, 2006). These parameters depend on the aerosol scattering and absorption coefficients and the mass concentration of specific components, thus linking the aerosol chemical and optical properties of climate-relevant species. Therefore, they are very useful to better parameterize the direct radiative effect of aerosols in atmospheric models (Hand and Malm, 2007; Seinfeld and Pandis, 2016). The MSEs and MAEs of different chemical aerosol components have been extensively reported (Hand and Malm, 2007; Caponi et al., 2017). MSE and MAE values for specific aerosol sources can also be found in the literature (Ealo et al., 2018; Forello et al., 2020). Knowledge of both MSEs and MAEs enables the investigation of the relationship between the sources contributing to air quality degradation and their potential to absorb and scatter light (Ealo et al., 2018). In order

* Corresponding author. Aguilera Laboratory of Atmospheric Pollution, Miguel Hernández University, Av. de la Universidad s/n, Edif. Alcudia, 03202, Elche, Spain.
E-mail address: j.nicolas@umh.es (J.F. Nicolás).

https://doi.org/10.1016/j.jastp.2025.106698
Received 14 October 2025; Received in revised form 27 November 2025; Accepted 29 November 2025
Available online 2 December 2025

to obtain the contribution of different aerosol sources to light absorption and scattering, the multiple linear regression (MLR) method is usually used. In this approach, source contributions obtained by means of techniques such as PMF (positive matrix factorization) or PCA (principal components analysis) are used as dependent variables. The use of multivariate receptor models is a robust approach for performing optical source apportionment (Bhardwaj and Raman, 2024). An important characteristic of the PMF/PCA factors is that they consider the internal mixing of atmospheric particles (Ealo et al., 2018).

The single scattering albedo (SSA) is a key parameter to determine whether aerosols cool or warm the Earth-atmosphere system over a specific region (Titos et al., 2012). SSA is defined as the ratio of aerosol light scattering to aerosol light extinction. For non-absorbing aerosols the SSA is ~1 (Eun Chu et al., 2016; Rajesh and Ramachandran, 2020). Values approaching 1 may be observed at certain Antarctic stations that are minimally affected by pollution from surrounding regions (Filonchyk et al., 2025). Values below 0.85 are associated with highly absorbing particles (Schmeisser et al., 2017; Romano et al., 2019). Therefore, obtaining information on the aerosol SSA is crucial, since the sensitivity of aerosol direct radiative forcing is primarily driven by differences in SSA values (Abel et al., 2005; Magi et al., 2008). Both the SSA and its spectral dependence may help to characterise the types of aerosols or aerosol sources in a certain environment (Costabile et al., 2013). For instance, SSA values are high and increase with wavelength for dust aerosols, while BB aerosols typically exhibit lower SSA values that decrease with the wavelength (Russell et al., 2010; Denjean et al., 2020).

The main goals of the present research are: (1) to estimate the relative contribution of $PM_{2.5}$ (fine particulate matter) sources to light absorption and scattering in a rural environment located in southeastern Spain during wintertime, and (2) to determine the SSA and its spectral dependence as a function of the type of dominant aerosol. The findings may be useful for making future climate projections in the Mediterranean region more accurate.

2. Methodology

2.1. Measurement site and $PM_{2.5}$ chemical characterization

$PM_{2.5}$ samples were collected in Benejama (38° 42 N, 0° 46 W, 592 m.a.s.l), a small town located 45 km from the Mediterranean coast, in the southeast of the Iberian Peninsula. The measurement station, classified as a rural site, was located on the outskirts of the town as shown in Fig. S1 (supplementary material). The area is affected by BB emissions during the cold season and also by the transport of mineral dust from North Africa. A detailed description of the sampling site can be found in Gómez-Sánchez et al. (2024).

Twenty-four-hour $PM_{2.5}$ samples were collected daily between December 5, 2023 and March 5, 2024 by means of a MCV high-volume sampler (30 $m^3 \cdot h^{-1}$). Mass concentrations were determined by gravimetric analysis in an environmentally controlled chamber (temperature of 20 ± 1 °C and relative humidity of 50 ± 5 %). $PM_{2.5}$ samples were analysed for elemental and organic carbon (EC, OC), levoglucosan, elements and water-soluble ions. A complete description of the analytical procedures is provided elsewhere (Gómez-Sánchez et al., 2024). A summary of the analytical techniques is presented in Table 1.

2.2. Determination of aerosol optical properties

Scattering coefficients (σ_{sp}) at three wavelengths (450, 525 and 635 nm) were measured every 5 min with a LED-based integrating nephelometer (model Aurora 3000, ECOTECH Pty Ltd., Knoxfield, Australia) provided with a $PM_{2.5}$ inlet. Data were corrected for truncation errors and for the non-ideal (non-Lambertian) illumination function of the light source as described by Müller et al. (2011). The measurements were performed under dry aerosol conditions (RH < 40 %) by means of a processor-controlled automatic heater. Measurements of absorption coefficients (σ_{ap}) were performed using an aethalometer (model AE33, Magee Scientific, USA) equipped with a $PM_{2.5}$ inlet. The aethalometer provides the absorption coefficient at seven wavelengths (370, 470, 520, 590, 660, 880 and 950 nm). To obtain aerosol absorption coefficients from aerosol attenuation coefficients, the harmonization factor for M8060 filter tape (H* factor = 1.76) was used (Savadkoohi et al., 2023). The time resolution was 5 min. Daily averages of absorption and scattering coefficients were subsequently calculated.

Table 1
Analytical techniques used to determine the chemical composition of $PM_{2.5}$ samples.

Analysis	Filter punch	Tecnique	Equipe
Elemental	47 mm	ED-XRF[a]	ARL Quant'x Spectometer with Si(Li) detector
EC and OC	1.5 cm^2	Thermo-optical	Sunset Thermo-optical carbon Analyser[b]
Anions	8.7 cm^2	Ion chromatograpy	Dionex Aquion (AS11-HC column)
Cations	8.7 cm^2	Ion chromatograpy	Dionex ICS-1100 (CS12A column)
Levoglucosan	47 mm	HPAEC-PAD[c]	Dionex Integrion (Carbopac PA1 column)

[a] Energy Dispersive X-Ray Fluorescence.
[b] The EUSAAR 2 protocol was used.
[c] High-performance anion exchange chromatography with pulsed amperometric detection.

The following parameters were calculated from $\sigma_{sp,\lambda}$ and $\sigma_{ap,\lambda}$ values: absorption Ångström exponent (AAE), scattering Ångström exponent (SAE), and SSA. The following equations were used:

$$AAE = \frac{Ln\frac{\sigma_{ap,\lambda_1}}{\sigma_{ap,\lambda_2}}}{Ln\frac{\lambda_1}{\lambda_2}} \quad (1)$$

where λ_1 = 370 nm and λ_2 = 950 nm.

$$SAE = \frac{Ln\frac{\sigma_{sp,\lambda_1}}{\sigma_{sp,\lambda_2}}}{Ln\frac{\lambda_1}{\lambda_2}} \quad (2)$$

where λ_1 = 450 nm and λ_2 = 635 nm.

$$SSA_\lambda = \frac{\sigma_{sp,\lambda}}{\sigma_{sp,\lambda} + \sigma_{ap,\lambda}} \quad (3)$$

These intensive optical properties provide information on particle size (SAE), the chemical composition of absorbing aerosols (AAE) and how particles interact with incoming radiation (SSA).

2.3. Estimation of source contribution to aerosol absorption and scattering

First, the contribution of sources to $PM_{2.5}$ concentrations were obtained by principal component analysis (PCA). The components (or sources) obtained by this method were used as independent variables in the MLR model. The MLR analysis was performed when all the general assumptions were satisfied by the explanatory variables. The model is described by the following equation:

$$y = b_o + \sum_{i=1}^{k} a_i \cdot x_i + \varepsilon \quad (4)$$

where y is the output data to be predicted by the model (in this case, $PM_{2.5}$ concentrations), x_i are the independent input variables (in the present study, mass concentrations of the sources identified by PCA), a_i are the linear regression coefficients, b_0 is the y-intercept (constant term) and ε is the residual term.

Finally, to estimate the contribution of $PM_{2.5}$ sources to light

scattering and absorption from the results of PCA, the procedure was again applied considering $\sigma_{sp,525}$ and $\sigma_{ap,520}$ as dependent variables. The unstandardized regression coefficients of the model (a_i) correspond to the MAE and MSE values (in $m^2 \cdot g^{-1}$) of each source. The analysis was performed by means of the SPSS software.

2.4. Meteorological data

Meteorological variables were measured using a Davis Vantage Pro2 weather station located right next to the sampling site. Fig. S2a (supplementary material) shows the evolution of some meteorological parameters and the influence of Saharan dust outbreaks during the measurement campaign. Saharan dust episodes (SDEs) over the study area were identified by means of the MONARCH predictive model (dust.aemet.es/products/daily-dust-products) and the analysis of PM time series. In addition, the temporal variation of Ti was examined, as it serves as a reliable tracer of SDEs in the study area (Galindo et al., 2020; López-Caravaca et al., 2022). During the sampling period, three short-lived SDEs were recorded: SDE_1 (13–14 January 2024), SDE_2 (28–29 January 2024), and SDE_3 (6–8 February 2024). In each case, air masses loaded with mineral dust reached the sampling site under the influence of a high-pressure system centred over the northwestern sector of the African continent. These events are illustrated in the supplementary material (Fig. S2b).

3. Results

3.1. Overview of optical properties

Table 2 shows summary statistics of aerosol optical properties (AOPs) and $PM_{2.5}$ concentrations. It should be noted that %BB was obtained by applying the Aethalometer Model (Sandradewi et al., 2008) assuming that $AAE_{FF} = 1$ and $AAE_{BB} = 2$, and the SSA_{525} value was calculated after determining $\sigma_{ap,525}$ by interpolation.

Since the measurement campaign was conducted in winter, comparisons with other studies performed on an annual basis are not straight forward. Nevertheless, scattering coefficients were in the range of those obtained in European rural and regional stations. In contrast, the average SAE value was lower than those reported for other sites in Europe (Pandolfi et al., 2018; Suchánková et al., 2024). The most likely reason is the higher frequency of Saharan dust outbreaks in our study area. Alternatively, the absorption coefficient at 370 nm was also in the range of those found at suburban and regional stations of Europe (Rovira et al., 2025). The average AAE value suggests that, in addition to BC, BrC and mineral dust also contributed to light absorption. It is important to mention that the contribution of BB, considered as the main source of BrC (Washenfelder et al., 2015; Zhang et al., 2020), was significant during the measurement campaign (Table 2). Moreover, as previously mentioned, three SDEs over the study area were identified during the study period.

The values of the absorption and scattering coefficients measured during winter at a suburban site located ~60 km from Benejama were 26 % and 35 % higher, respectively, than those reported here (López-Caravaca et al., 2021), due to the more rural character of the area. On the other hand, the average SSA value (<0.85) points to a certain dominance of light-absorbing aerosols over the study region.

Fig. 1 shows the variability of daily values of AOPs and $PM_{2.5}$ concentrations. The evolution of $PM_{2.5}$, $\sigma_{ap,520}$ y $\sigma_{sp,525}$ was very similar. In fact, the correlation coefficients of $\sigma_{ap,520}$ and $\sigma_{sp,525}$ with $PM_{2.5}$ concentrations were higher than 0.9. MAE and MSE values derived from these correlations were 0.83 ± 0.03 $m^2 \cdot g^{-1}$ and 4.31 ± 0.13 $m^2 \cdot g^{-1}$, respectively.

The variability of AOPs and $PM_{2.5}$ concentrations was strongly influenced by meteorological conditions. The maximum values of $\sigma_{sp,525}$ (~100 Mm^{-1}) and $\sigma_{ap,520}$ (~25 Mm^{-1}) registered at the end of 2023 coincided with SAE and AAE values exceeding 1.6 and 1.5, respectively. These values were most likely the result of an increase in the levels of fine aerosols caused by high atmospheric stability conditions: a high-pressure system over the Iberian Peninsula and West Mediterranean, low wind speeds (Fig. S2) and a decrease in the mixing layer height. While scattering parameters and $PM_{2.5}$ levels peaked during Saharan dust events, absorption parameters ($\sigma_{ap,520}$ y AAE) were high only during the first episode. SAE values indicate that the end of SDE_1 and SDE_3 was characterized by an increase in the levels of coarse mode aerosols. However, this did not occur during SDE_2. On the other hand, the decrease in $PM_{2.5}$, $\sigma_{ap,520}$ and $\sigma_{sp,525}$ toward the end of the measurement period may be attributed to strong winds causing the dispersion of air pollutants (Fig. S2). During this period (from 23 to 28 February), SAE values significantly decreased, with average values lower than 1.0. The most likely reason is the increase in coarse PM concentrations as a result of wind-induced resuspension. SSA values were high during SDEs, with a maximum value of 0.93 during SDE_2.

Table 2
Summary statistics of daily $PM_{2.5}$ concentrations ($\mu g \cdot m^{-3}$), absorption and scattering coefficients at different wavelengths (Mm^{-1}), BC ($\mu g \cdot m^{-3}$), AAE, SAE and SSA (dimensionless) at the sampling site.

	Mean	SD	P5	Median	P95
$PM_{2.5}$	8.8	3.0	4.7	8.6	14.2
$\sigma_{sp,450}$	44.5	26.8	11.6	39.1	101.3
$\sigma_{sp,525}$	35.0	20.6	9.5	29.6	77.4
$\sigma_{sp,635}$	27.3	15.0	8.2	23.6	56.7
$SAE_{(450-635)}$	1.235	0.404	0.467	1.345	1.729
$\sigma_{ap,370}$	13.1	7.2	3.9	12.7	24.0
$\sigma_{ap,440}$	9.5	5.1	2.9	9.0	17.2
$\sigma_{ap,520}$	7.5	4.0	2.2	7.1	13.5
$\sigma_{ap,590}$	6.1	3.2	1.8	5.7	11.0
$\sigma_{ap,660}$	5.1	2.7	1.4	4.8	9.1
$\sigma_{ap,880}$	3.6	1.9	1.0	3.4	6.6
$\sigma_{ap,950}$	3.3	1.7	0.9	3.2	6.0
$AAE_{(370-950)}$	1.450	0.107	1.265	1.437	1.609
%BB	38.2	6.2	29.4	37.7	50.3
BC_{880}	0.80	0.42	0.22	0.76	1.46
SSA_{525}	0.82	0.04	0.74	0.81	0.89

3.2. Source contributions to $PM_{2.5}$

The mean $PM_{2.5}$ chemical composition during the study period is shown in Table S1. The average levoglucosan concentration (0.137 $\mu g \cdot m^{-3}$) was two times higher than the value registered for PM_{10} at the same sampling site during late winter 2023 (Gómez-Sánchez et al., 2024), indicating a significant contribution from BB to $PM_{2.5}$ during the measurement period. In order to help the identification of aerosol sources, OC was divided into OC from BB (OC_{BB}) and OC emitted from other sources (OC_{NON-BB}). For this, OC/levoglucosan ratios at the sampling site were optimized using the method described by Nirmalkar et al. (2020). The procedure is depicted in detail in Clemente et al. (2024). A ratio of 9 was used. The correlation between OC_{NON-BB} and levoglucosan concentrations is shown in Fig. S3.

$PM_{2.5}$ sources were identified using PCA with Varimax rotation. According to the Kaiser criterion ($\lambda > 1$), five components (PC_1-PC_5) were selected. These components explained 83.3 % of the total variance (Table 3).

Principal components from PCA were attributed to the following sources.

- PC_1 was highly loaded with ammonium, sulfate, nitrate and oxalate and, therefore, it may be considered as a secondary aerosol formation source (SA).
- The second factor was attributed to biomass burning (BB) since it was dominated by OC_{BB}, EC and K^+.
- Factor 3 had high loadings of Ti, Fe and Ca and was identified as a mineral dust source (MD), including Saharan dust.

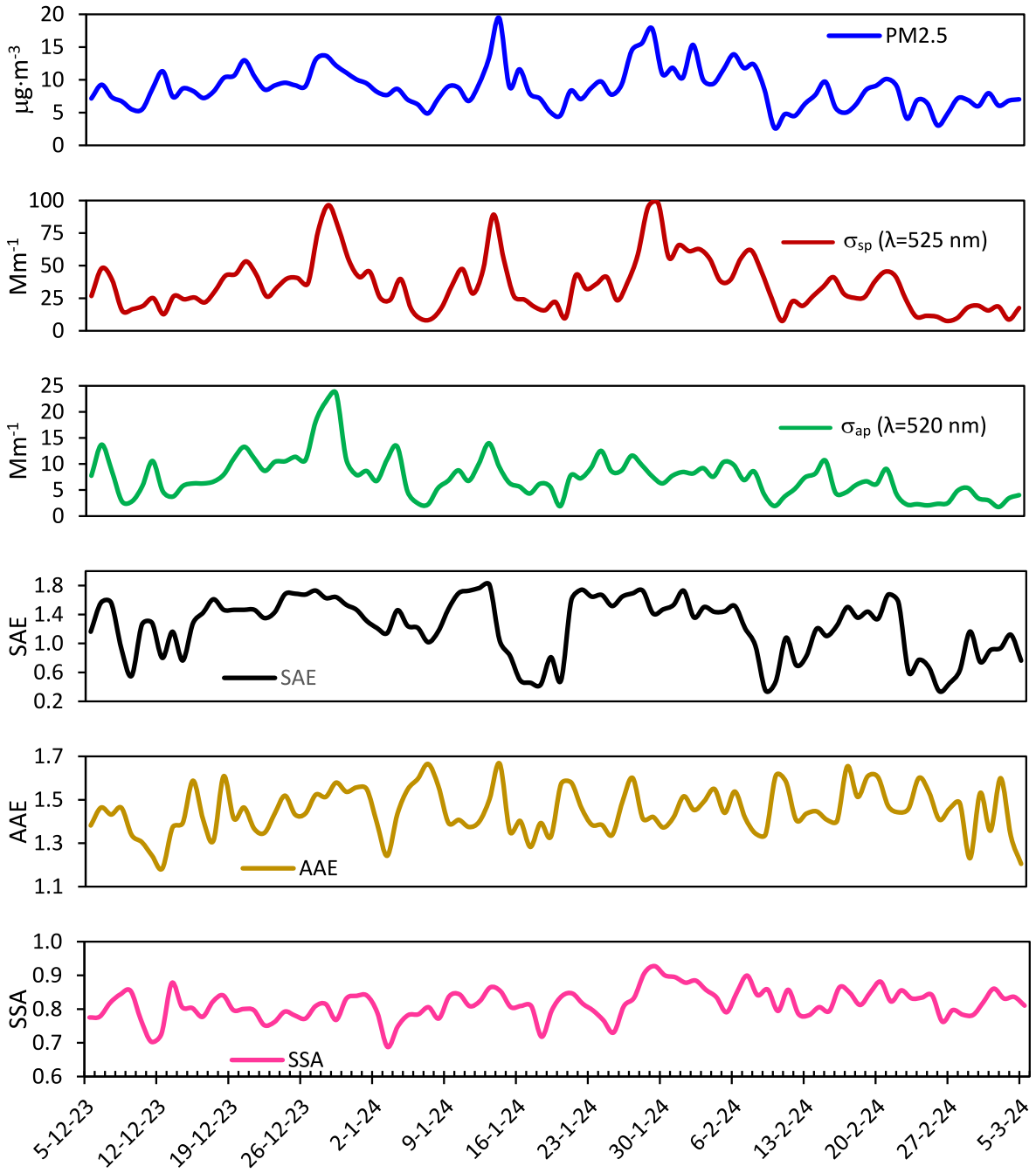

Fig. 1. Time series of daily $PM_{2.5}$ concentrations and aerosol optical properties.

- PC_4, with high loadings of sea-salt species, represents the marine aerosol source (MA).
- Finally, the fifth component was strongly loaded with Zn, EC and $OC_{NON\text{-}BB}$ and thus was identified as a traffic source (TR).

A PMF analysis was also performed in order to ensure the robustness of the source apportionment. Details about the choice of the PMF solution are provided in the Supplementary Material (SM-PMF solution). The sources identified were the same as those obtained from the PCA, and their contributions to $PM_{2.5}$ differed only slightly (discrepancies did not exceed 7 %). Therefore, the initial solution was considered acceptable. The R^2 values of the linear regression between the source contributions estimated by both methods were: $R^2(SA) = 0.86$, $R^2(BB) = 0.97$, $R^2(MD) = 0.82$, $R^2(MA) = 0.95$ and $R^2(TR) = 0.74$.

In order to quantify the contribution of sources to $PM_{2.5}$ concentrations, the MLR analysis was applied. $PM_{2.5}$ concentrations were the dependent variable and the five components obtained from the PCA were the independent variables. The results are presented in Table S2. The highest standardized coefficients were observed for SA, BB and MD, indicating that these components were the main contributors to the variability of $PM_{2.5}$ concentrations. Source contributions were estimated by multiplying the linear regression coefficients by the mass concentrations. The average contribution from each source to $PM_{2.5}$ is shown in Fig. 2. The figure also presents the variability of source contributions during the measurement period.

The contributions from the identified sources were similar, except that of MA. The lower contribution from this source to $PM_{2.5}$ concentrations can be explained by the distance of the sampling site to the Mediterranean coast and to the fact that sea salt particles are mainly distributed in the coarse mode. The contribution from MD depends on

Table 3
Varimax rotated factor loadings obtained by PCA.

	PC_1	PC_2	PC_3	PC_4	PC_5
Na^+	0.293	−0.138	−0.027	**0.902**	−0.082
NH_4^+	**0.931**	0.121	−0.112	0.007	−0.115
K^+	**0.636**	**0.337**	0.292	0.139	0.375
Mg^{2+}	0.178	−0.058	0.393	**0.778**	0.172
Ca^{2+}	−0.161	0.185	**0.750**	0.138	**0.383**
Cl^-	−0.089	−0.013	0.199	**0.873**	0.028
NO_3^-	**0.591**	**0.538**	0.248	0.030	−0.146
SO_4^{2-}	**0.929**	−0.009	0.014	0.210	0.010
$C_2O_4^{2-}$	**0.784**	0.071	0.268	0.099	0.331
EC	0.126	**0.757**	0.202	−0.190	**0.438**
Ti	0.162	0.024	**0.938**	0.147	−0.002
Fe	0.196	−0.022	**0.917**	0.187	−0.021
Zn	−0.056	0.390	−0.033	0.179	**0.690**
OC_{BB}	0.087	**0.972**	−0.023	−0.055	0.074
OC_{NONBB}	0.504	−0.083	0.297	−0.184	**0.652**
Eigenvalues	5.7	3.3	2.4	1.4	1.1
Explained variance (%)	35.4	20.2	14.7	8.7	4.3

The components with the highest loadings are marked in bold.

the frequency and intensity of Saharan dust outbreaks. Therefore, the contribution from this source to $PM_{2.5}$ levels at rural stations may vary considerably, depending on the geographic location of the sampling site. For instance, at rural stations of France the MD source accounted for less than 10 % of $PM_{2.5}$ concentrations (Font et al., 2024), while contributions higher than 30 % were reported in Crete (Greece) (Chatoutsidov and Lazaridis, 2022). Since mineral dust outbreaks vary in both frequency and intensity, the contribution from this source to $PM_{2.5}$ showed large variations. At rural sites, the contribution from BB can vary depending on the proxy method used (Font et al., 2022) or the climatic and geographical conditions. In the present study, the BB contribution was in the range of annual values found at different rural sites in France (17 %–27 %; Font et al., 2024) and Poland (21 %-winter average) (Kristensson et al., 2020). However, this contribution was slightly lower than those found in Northern Italy (27–31 %, fall and winter values) (Perrone et al., 2012), and clearly lower than those recorded in the Carpathian basin (Hungary), with values reaching 68 % in winter (Vörösmarty et al., 2023). Regarding the secondary source, its contribution was lower than those reported for rural stations of Europe (Scerri et al., 2019; Font et al., 2024).

3.3. Source contribution to absorption and scattering

MSE and MAE values for each source were evaluated by applying the MLR model to $\sigma_{sp,525}$ and $\sigma_{ap,520}$. Since the MLR model can be very sensitive to the selection of the variables included in the analysis (Hand and Malm, 2007), only MD, BB, RT and SA were considered. Since the contribution of MA to the average $PM_{2.5}$ concentration was lower than 10 %, attempts to include this factor in the model resulted in unrealistic mass absorption/scattering efficiencies and statistically non-significant regression coefficients for absorption and scattering (Ponczek et al., 2022). The results of the MLR analysis are shown in Table 4. Unstandardized coefficients represent MAE and MSE values for each source. All MSE and MAE values were statistically significant ($p < 0.05$).

As can be observed, SA and BB were the most contributing sources to light scattering, while BB was the factor that accounted for the largest fraction of the variability of $\sigma_{ap,520}$, followed by the traffic source. MD was the component with the lowest coefficients and, therefore, represents the source with the lowest scattering and absorption efficiencies. The average contribution from each source to $\sigma_{sp,525}$ and $\sigma_{ap,520}$ is shown in Fig. 3. The correlation between modelled and measured $\sigma_{sp,525}$ and $\sigma_{ap,520}$ is presented in Fig. S4.

BB accounted for almost half of aerosol absorption and made a significant contribution to scattering. The increase of absorption and scattering during BB events has been frequently reported (Palacios et al., 2022). The absorption associated to BB aerosols can be attributed, in addition to BC, to BrC emitted or formed during biomass combustion. The traffic source did not significantly contribute to $\sigma_{sp,525}$, but it accounted for 26 % of $\sigma_{ap,520}$ due to BC emissions from diesel and gasoline engines. MD showed the lowest contributions to both the absorption and scattering coefficients, comparable to those registered at the regional background station of Montseny, located in the northwest of the Iberian Peninsula (Ealo et al., 2018). Despite this, the daily contributions from MD to light absorption and scattering increased significantly during SDEs. For instance, during SDE_1, daily contributions of 49 % to $\sigma_{ap,520}$ and 37 % to $\sigma_{sp,525}$ were reached. These contributions were also elevated on days with high wind speeds. The secondary source made the greatest contribution to the scattering coefficient due to the presence of light scattering species in this factor, mainly $(NH_4)_2SO_4$ and NH_4NO_3. The contribution of this source to light scattering also increased during SDEs, most likely due to the formation of ammonium sulfate and nitrate on mineral dust particles (Galindo et al., 2008, 2020). The SA source contributed ~41 % to light extinction ($\sigma_{sp}+\sigma_{ap}$) at 525 nm. This percentage is lower than the joint contribution of $(NH_4)_2SO_4$ and NH_4NO_3 reported for urban background stations in Europe: 52 % at 550 nm in Milan (Italy; Valentini et al., 2018) and 50 % at 525 nm in Lille (France; Velazquez-García et al., 2023). In these cases, the contribution of NH_4NO_3 was clearly higher than that of $(NH_4)_2SO_4$.

3.4. SSA for different aerosol types

SSA values (± standard errors) for the identified sources were: SA (0.93 ± 0.17), BB (0.79 ± 0.13), MD (0.80 ± 0.19) and RT (0.60 ± 0.07). Fig. 4 shows the contribution of $PM_{2.5}$ sources for different SSA intervals. The number of samples for each interval (N) is as follows: 0.70–0.75: N = 7; 0.75–0.80: N = 28; 0.80–0.85: N = 39; 0.85–0.90: N = 14 and 0.90–0.95: N = 4.

SSA increased as the contribution of SA increased, reaching values

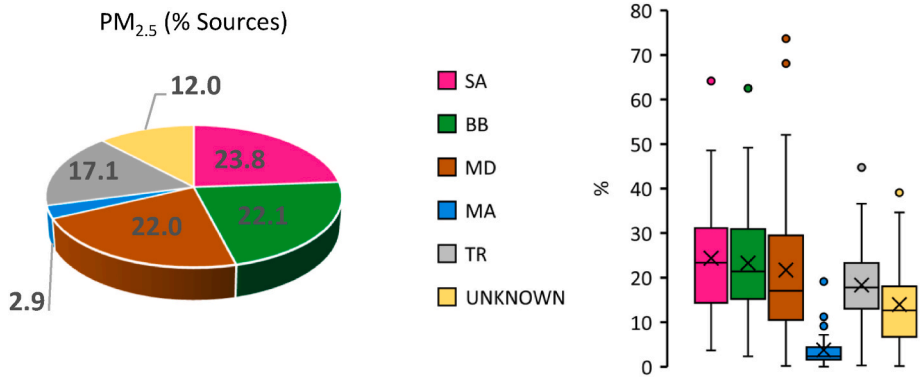

Fig. 2. Average percentage contributions to $PM_{2.5}$ of the PCA factors. Variability of the contributions are also shown.

Table 4
Results from the multilinear regression analysis between $\sigma_{sp,525}$ and $\sigma_{ap,520}$, and PCA factors.

Source	Unstandardized coefficients (B) ($m^2 \cdot g^{-1}$)	Std. error ($m^2 \cdot g^{-1}$)	Standardized coefficients	p-value	95 % Confidence Interval for B (LB-UB)	R^2
$\sigma_{sp,525}$						0.93
SA	11.87	0.519	0.530	0.000	10.84–12.91	
BB	9.24	0.510	0.431	0.000	8.22–10.26	
MD	2.02	0.542	0.077	0.000	0.94–3.11	
TR	1.53	0.453	0.087	0.001	0.26–2.44	
$\sigma_{ap,520}$						0.83
SA	0.93	0.147	0.197	0.000	0.63–1.22	
BB	2.48	0.144	0.554	0.000	2.19–2.77	
MD	0.52	0.154	0.094	0.001	0.21–0.83	
TR	1.00	0.128	0.273	0.000	0.74–1.26	

UB: Upper Bound; LB: Lower Bound.

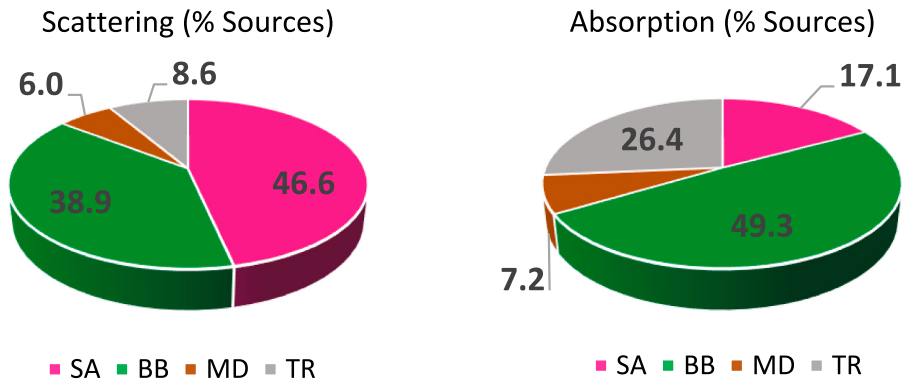

Fig. 3. Average percentage contributions to $\sigma_{sp,525}$ and $\sigma_{ap,520}$ of $PM_{2.5}$ sources.

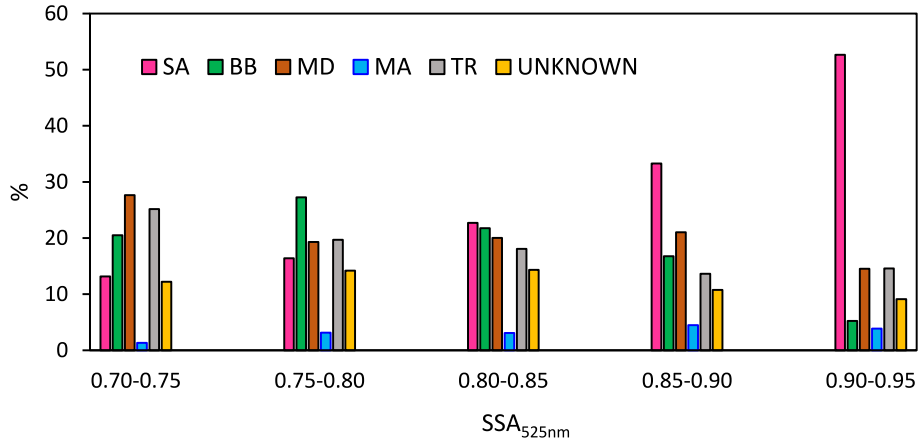

Fig. 4. Percentage contributions of the identifies sources to $PM_{2.5}$ concentrations as a function of SSA ranges.

higher than 0.85 when the contribution from this source to $PM_{2.5}$ concentrations was greater than 30 %. The reason is the presence of light-scattering aerosol components in this source, as stated above. As expected, the traffic source showed an opposite trend, while the marine aerosol source peaked in the 0.85–0.90 interval. The contribution of BB to $PM_{2.5}$ concentrations was fairly constant for all SSA intervals, except for the 0.90–0.95 range, for which the contribution of this source was significantly lower. SSA values reported in the literature for this type of aerosol are highly variable, ranging from 0.80 to 0.87 at 532 nm (Spain; Alados-Arboledas et al., 2011) and 0.71–0.77 at 550 nm (West Africa; Denjean et al., 2020). The reason for this high variability is that the optical properties of BB aerosols depend on burning conditions and the type of biomass burned. The contribution of MD to $PM_{2.5}$ levels was similar (~20 %) for SSA values between 0.75 and 0.90. Nevertheless, this contribution decreased to 14.5 % for higher SSA values. Regarding this source, it is important to mention that, during SDEs (N = 7), the contribution of MD to $PM_{2.5}$ concentrations notably increased for high SSA values, being 48.4 %, 57.9 % and 23.6 % for the 0.80–0.85, 0.85–0.90 and 0.90–0.95 intervals, respectively. This was expected since SSA values in the western Mediterranean during SDEs are usually higher than 0.88 (Denjean et al., 2016; Castañer et al., 2017).

Fig. 5 shows SSA values for different wavelengths as a function of aerosol sources. Only SSA data for daily source contributions higher than the 95 percentile (N = 7) were considered. The selection of such a high percentile was made to ensure that each source type predominated in the samples used to represent Fig. 5. P95 values were: SA (39.0 %), MD (39.0 %), BB (38.2 %), TR (26.3 %) and MA (8.0 %). For the MD source, five out of seven days were under the influence of SDE. Using this

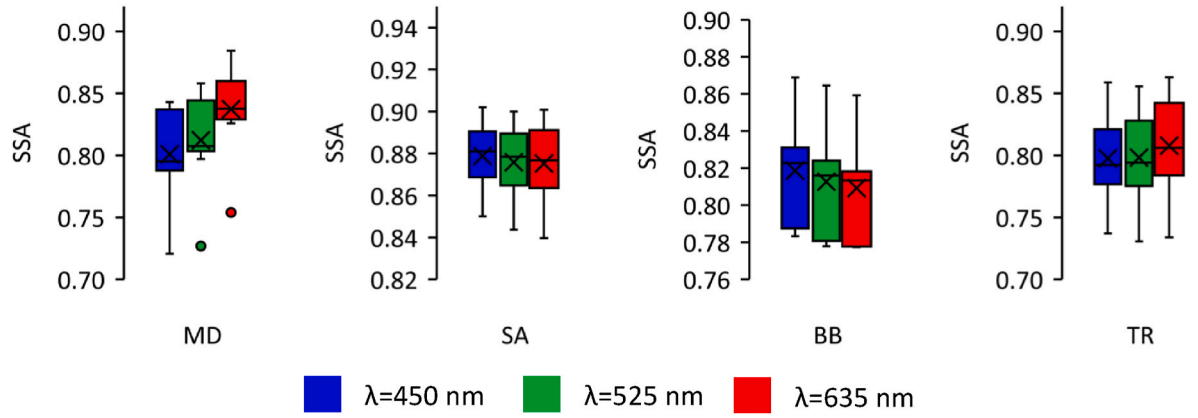

Fig. 5. SSA spectral variation according to aerosol type.

criterion, each set of samples can be considered to represent one type of aerosol, except the marine aerosol. Table S3 shows the contribution of each source to $PM_{2.5}$ concentrations as a function of the dominant aerosol type. For instance, the MD source contributed ~54 % to this type of aerosol, while only 12 % of the aerosol classified as "marine" originated from this source. For this reason, the MA has not been included in Fig. 5.

For the MD aerosol, the SSA increased with the increase in wavelength, as reported in previous works (Denjean et al., 2020; López-Caravaca et al., 2021). The most likely reason is that dust particles are mainly coarse particles; consequently, scattering remains relatively constant as a function of wavelength, and the single scattering albedo follows the decrease in absorption with wavelength (Bergstrom et al., 2007). In contrast, for BB aerosols, SSA values decreased with increasing wavelength (Denjean et al., 2020; Boselli et al., 2021) since scattering for fine particles often decreases faster than absorption (Bergstrom et al., 2007). At our sampling site, a smooth decrease was observed. The SSA of the secondary aerosol source did not show a clear spectral dependence since it is mainly made of hygroscopic particles, such as sulfates (Dubovik et al., 2002). SSA values for the aerosol classified as "traffic" were similar for the three wavelengths, most likely because the TR source contributed only ~33 % to this type of aerosol (see Table S3) and, therefore, it likely represents a mix of aerosol types.

4. Conclusions

From the results obtained, four main conclusions can be drawn.

- The mass contribution of the identified $PM_{2.5}$ sources does not always reflect their relative impact on light scattering and absorption. A notable example is the biomass burning source, whose contribution to $PM_{2.5}$ mass concentrations was roughly half of its effect on $\sigma_{sp,525}$ and $\sigma_{ap,520}$ values.
- Within the MD source, local and Saharan (MD_{SDE}) components must be distinguished. MD_{SDE} contributed more strongly to both scattering and absorption. Furthermore, the contribution of MD to $PM_{2.5}$ during SDEs increased significantly for high SSA values.
- Variability in $PM_{2.5}$ source contributions had a substantial influence on SSA values. SSA increased with higher contributions from the secondary source. Indeed, SSA values exceeding 0.85 were observed when the contribution from the secondary source was higher than 33 %. Conversely, the traffic source showed the opposite trend, with SSA decreasing as its contribution increased.
- Anthropogenic sources (biomass burning, traffic, and secondary aerosols), which are the main contributors to air quality deterioration, had the strongest influence on light extinction in the southwestern Mediterranean.

CRediT authorship contribution statement

J.F. Nicolás: Writing – original draft, Supervision, Investigation, Funding acquisition, Formal analysis. **J. Crespo:** Validation, Supervision, Conceptualization. **E. Yubero:** Writing – review & editing, Project administration, Funding acquisition. **M. Alfosea-Simón:** Investigation, Formal analysis. **A. Clemente:** Investigation, Formal analysis. **N. Gómez-Sanchez:** Investigation, Formal analysis. **N. Galindo:** Writing – review & editing, Project administration, Funding acquisition.

Declaration of competing interest

The authors declare that they have no known competing financial interests or personal relationships that could have appeared to influence the work reported in this paper.

Acknowledgements

This work was supported by: MCIN/AEI/10.13039/501100011033 and the "European Union NextGenerationEU/PRTR" (CAMBIO project, ref. TED2021-131336B–I00); MICIU/AEI/10.13039/501100011033 and by FEDER, EU (TOXICAR project, ref. PID2023-149608OB-I00), and the Valencian Regional Government (Generalitat Valenciana, CIAICO/2024/301 research project). The authors would like to thank AVAMET for supplying meteorological data and the ACTRIS-Spain network (CGL2017-90884-REDT).

Appendix A. Supplementary data

Supplementary data to this article can be found online at https://doi.org/10.1016/j.jastp.2025.106698.

Data availability

Data will be made available on request.

References

Abel, S.J., Highwood, E.J., Haywood, J.M., Stringer, M.A., 2005. The direct radiative effect of biomass burning aerosols over Southern Africa. Atmos. Chem. Phys. 5, 1999–2018. https://doi.org/10.5194/acp-5-1999-2005.

Alados-Arboledas, L., Müller, D., Guerrero-Rascado, J.L., Navas-Guzmán, F., Pérez-Ramírez, D., Olmo, F.J., 2011. Optical and microphysical properties of fresh biomass burning aerosol retrieved by Raman lidar, and star-and sun-photometry. Geophys. Res. Lett. 38, L01807. https://doi.org/10.1029/2010GL045999.

Bergstrom, R.W., Pilewskie, P., Russell, P.B., Redemann, J., Bond, T.C., Quinn, P.K., Sierau, B., 2007. Spectral absorption properties of atmospheric aerosols. Atmos. Chem. Phys. 7, 5937–5943. https://doi.org/10.5194/acp-7-5937-2007, 2007.

Bhardwaj, A., Raman, R.S., 2024. Sources of atmospheric light-absorbing fine aerosols: insights from optical source apportionment utilizing measurements made during

COVID-19 lockdowns at a COALESCE network site - bhopal, India. Atmos. Environ. 321, 120343. https://doi.org/10.1016/j.atmosenv.2024.120343.
Bond, T.C., Bergstrom, R.W., 2006. Light absorption by carbonaceous particles: an investigative review. Aerosol Sci. Technol. 40 (1), 27–67. https://doi.org/10.1080/02786820500421521.
Boselli, A., Sannino, A., D'Emilio, M., Wang, X., Amoruso, S., 2021. Aerosol characterization during the summer 2017 huge fire event on Mount Vesuvius (Italy) by remote sensing and in situ observations. Remote Sens. 13, 2001. https://doi.org/10.3390/rs13102001.
Caponi, L., Formenti, P., Massabó, D., Di Biagio, C., Cazaunau, M., Pangui, E., Chevaillier, S., Landrot, G., Andreae, M.O., Kandler, K., Piketh, S., Saeed, T., Seibert, D., Williams, E., Balkanski, Y., Prati, P., Doussin, J.-F., 2017. Spectral- and size-resolved mass absorption efficiency of mineral dust aerosols in the shortwave spectrum: a simulation chamber study. Atmos. Chem. Phys. 17, 7175–7191. https://doi.org/10.5194/acp-17-7175-2017.
Castañer, R., Nicolás, J.F., Crespo, J., Yubero, E., Galindo, N., Caballero, S., Pastor, C., 2017. Influence of air mass origins on optical properties and PM concentrations measured at a high mountain station located in the southwestern Mediterranean. Atmos. Res. 197, 244–254. https://doi.org/10.1016/j.atmosres.2017.07.013.
Chatoutsidou, S.E., Lazaridis, M., 2022. Mass concentrations and elemental analysis of $PM_{2.5}$ and PM_{10} in a coastal Mediterranean site: a holistic approach to identify contributing sources and varying factors. Sci. Total Environ. 838, 155980. https://doi.org/10.1016/j.scitotenv.2022.155980.
Clemente, A., Yubero, E., Nicolás, J.F., Crespo, J., Galindo, N., 2024. Organic tracers in fine and coarse aerosols at an urban Mediterranean site: contribution of biomass burning and biogenic emissions. Environ. Sci. Poll. Res. 31, 25216–25226. https://doi.org/10.1007/s11356-024-32789-x.
Costabile, F., Barnaba, F., Angelini, F., Gobbi, G.P., 2013. Identification of key aerosol populations through their size and composition resolved spectral scattering and absorption. Atmos. Chem. Phys. 13, 2455–2470. https://doi.org/10.5194/acp-13-2455-2013.
Denjean, C., Cassola, F., Mazzino, A., Triquet, S., Chevaillier, S., Grand, N., Bourrianne, T., Momboisse, G., Sellegri, K., Schwarzenbock, A., Freney, E., Mallet, M., Formenti, P., 2016. Size distribution and optical properties of mineral dust aerosols transported in the western Mediterranean. Atmos. Chem. Phys. 16, 1081–1104. https://doi.org/10.5194/acp-16-1081-2016.
Denjean, C., Bourrianne, T., Burnet, F., Mallet, M., Maury, N., Colomb, A., Dominutti, P., Brito, J., Dupuy, R., Sellegri, K., Schwarzenboeck, A., Flamant, C., Knippertz, P., 2020. Overview of aerosol optical properties over southern West Africa from DACCIWA aircraft measurements. Atmos. Chem. Phys. 20, 4735–4756. https://doi.org/10.5194/acp-20-4735-2020.
Dubovik, O., Holben, B.N., Eck, T.F., Smirnov, A., Kaufman, Y.J., King, M.D., Tanre, D., Slutsker, I., 2002. Variability of absorption and optical properties of key aerosol types observed in worldwide locations. J. Atmos. Sci. 59, 590–608. https://doi.org/10.1175/1520-0469(2002)059<0590:VOAAOP>2.0.CO;2.
Ealo, M., Alastuey, A., Pérez, N., Ripoll, A., Querol, X., Pandolfi, M., 2018. Impact of aerosol particle sources on optical properties in urban, regional and remote areas in the north-western Mediterranean. Atmos. Chem. Phys. 18, 1149–1169. https://doi.org/10.5194/acp-18-1149-2018.
Filonchyk, M., Peterson, M.P., Hurynovich, V., Zhang, L., He, Y., 2025. Aerosol composition and properties in Antartica: optical, microphysical and radiative characteristics. Glob. Planet. Change. 253, 104935. https://doi.org/10.1016/j.gloplacha.2025.104935.
Font, A., Ciupek, K., Butterfield, D., Fuller, G.W., 2022. Long-term trends in particulate matter from wood burning in the United Kingdom: dependence on weather and social factors. Environ. Poll. 314, 120105. https://doi.org/10.1016/j.envpol.2022.120105.
Font, A., de Brito, J.F., Riffault, V., Conil, S., Jaffrezo, J.-L., Bourin, A., 2024. Long-term measurements of aerosol composition at rural background sites in France: sources, seasonality and mass closure of $PM_{2.5}$. Atmos. Environ. 334, 120724. https://doi.org/10.1016/j.atmosenv.2024.120724.
Forello, A.C., Amato, F., Bernardoni, V., Calzolai, G., Canepari, S., Costabile, F., Liberto, L.D., Gualtieri, M., Lucarelli, F., Nava, S., Perrino, C., Petralia, E., Valentini, S., Valli, G., Vecchi, R., 2020. Gaining knowledge on source contribution to aerosol optical absorption properties and organics by receptor modelling. Atmos. Environ. 243, 117873. https://doi.org/10.1016/j.atmosenv.2020.117873.
Galindo, N., Nicolás, J.F., Yubero, E., Caballero, S., Pastor, C., Crespo, J., 2008. Factors affecting levels of aerosol sulfate and nitrate on the Western Mediterranean coast. Atmos. Res. 88, 5–313. https://doi.org/10.1016/j.atmosres.2007.11.024.
Galindo, N., Yubero, E., Clemente, A., Nicolás, J.F., Varea, M., Crespo, J., 2020. PM events and changes in the chemical composition of urban aerosols: a case study in the western Mediterranean. Chemosphere 244, 125520. https://doi.org/10.1016/j.chemosphere.2019.125520.
Gómez-Sánchez, N., Galindo, N., Alfosea-Simón, M., Nicolás, J.F., Crespo, J., Yubero, E., 2024. Chemical composition of PM_{10} at a rural site in the western Mediterranean and its relationship with the oxidative potential. Chemosphere 363, 142880. https://doi.org/10.1016/j.chemosphere.2024.142880.
Hand, J.L., Malm, W.C., 2007. Review of aerosol mass scattering efficiencies from groundbased measurements since 1990. J. Geophys. Res. 112, D16203. https://doi.org/10.1029/2007JD008484.
Kristensson, A., Ausmeel, S., Pauraite, J., Eriksson, A., Ahlberg, E., Bycenkiene, S., Degórska, A., 2020. Source contributions to rural carbonaceous winter aerosol in North-Eastern Poland. Atmosphere 11, 1–19. https://doi.org/10.3390/atmos11030263.
Lelieveld, J., Klingmüller, K., Pozzer, A., Burnett, R.T., Haines, A., Ramanathan, V., 2019. Effects of fossil fuel and total anthropogenic emission removal on public health and climate. Proc. Natl. Acad. Sci. 116, 7192–7197. https://doi.org/10.1073/pnas.1819989116.
Li, J., Carlson, B.E., Yung, Y.L., Lv, D., Hansen, J., Penner, J.E., Liao, H., Ramaswamy, V., Kahn, R.A., Zhang, P., Dubovik, O., Ding, A., Lacis, A.A., Zhang, L., Yueming Dong, Y., 2022. Scattering and absorbing aerosols in the climate system. Nat. Rev. Earth Environ. 3, 363–379. https://doi.org/10.1038/s43017-022-00296-7.
López-Caravaca, A., Castañer, R., Clemente, A., Yubero, E., Galindo, N., Crespo, J., Nicolás, J.F., 2021. The impact of intense winter saharan dust events on PM and optical properties at urban sites in the southeast of the Iberian Peninsula. Atmosphere 12, 1469. https://doi.org/10.3390/atmos12111469.
López-Caravaca, A., Nicolás, J.F., Lucarelli, F., Castañer, R., Crespo, J., Galindo, N., Calzolai, G., Yubero, E., Clemente, A., Pazzi, G., 2022. Combination of PM optical and chemical properties to estimate the contribution of non-BC absorbers to light absorption at a remote site. Atmos. Res. 268, 106000. https://doi.org/10.1016/j.atmosres.2021.106000.
Magi, B.I., Fu, Q., Redemann, J., Schmid, B., 2008. Using aircraft measurements to estimate the magnitude and uncertainty of the shortwave direct radiative forcing of southern African biomass burning aerosol. J. Geophys. Res. 113, D05213. https://doi.org/10.1029/2007JD009258, 20081.
Moosmüller, H., Chakrabarty, R.K., Arnott, W.P., 2009. Aerosol light absorption and its measurement: a review. J. Quant. Spectrosc. Radiat. Transf. 110, 844–878. https://doi.org/10.1016/j.jqsrt.2009.02.035.
Müller, T., Laborde, M., Kassel, G., Wiedensolher, A., 2011. Design and performance of a three-wavelength LED-based total scatter and backscatter integrating nephelometer. Atmos. Meas. Tech. 4, 1291–1303. https://doi.org/10.5194/amtd-3-4835-2010.
Nirmalkar, J., Batmunkh, T., Jung, J., 2020. An optimized tracer-based approach for estimating organic carbon emissions from biomass burning in Ulaanbaatar, Mongolia. Atmos. Chem. Phys. 20, 3231–3247. https://doi.org/10.5194/acp-20-3231-2020, 2020.
Palacios, R., Romera, K., Rizzo, L., Cirino, G., Adams, D., Imbiriba, B., Nassarden, D., Rothmund, L., Siqueira, A., Basso, J., Rodrigues, T., Curado, L., Weber, A., Nogueira, J., Morais, F., Artaxo, P., 2022. Optical properties and spectral dependence of aerosol light absorption over the Brazilian Pantanal. Atmos. Pollut. Res. 13, 101413. https://doi.org/10.1016/j.apr.2022.101413.
Pandolfi, M., Alados-Arboledas, L., Alastuey, A., Andrade, M., Angelov, C., Artiñano, B., Backman, J., Baltensperger, U., Bonasoni, P., Bukowiecki, N., Collaud Coen, M., Conil, S., Coz, E., Crenn, V., Dudoitis, V., Ealo, M., Eleftheriadis, K., Favez, O., Fetfatzis, P., Fiebig, M., Flentje, H., Ginot, P., Gysel, M., Henzing, B., Hoffer, A., Holubova Smejkalova, A., Kalapov, I., Kalivitis, N., Kouvarakis, G., Kristensson, A., Kulmala, M., Lihavainen, H., Lunder, C., Luoma, K., Lyamani, H., Marinoni, A., Mihalopoulos, N., Moerman, M., Nicolas, J., O'Dowd, C., Petäjä, T., Petit, J.-E., Pichon, J.M., Prokopciuk, N., Putaud, J.-P., Rodríguez, S., Sciare, J., Sellegri, K., Swietlicki, E., Titos, G., Tuch, T., Tunved, P., Ulevicius, V., Vaishya, A., Vana, M., Virkkula, A., Vratolis, S., Weingartner, E., Wiedensohler, A., Laj, P., 2018. A European aerosol phenomenology – 6: scattering properties of atmospheric aerosol particles from 28 ACTRIS sites. Atmos. Chem. Phys. 18, 7877–7911. https://doi.org/10.5194/acp-18-7877-2018.
Pani, S.K., Lin, N.-H., Wang, S.-H., Chantara, S., Stephen, M., Griffith, S.M., Jackson Chang, J., 2023. Aerosol mass scattering efficiencies and single scattering albedo under high mass loading in Chiang Mai valley, Thailand. Atmos. Environ. 308, 119867. https://doi.org/10.1016/j.atmosenv.2023.119867.
Pérez-Vizcaíno, P., Sánchez de la Campa, A.M., Sánchez-Rodas, D., Alastuey, A., Querol, X., de la Rosa, J., 2026. PM_{10} chemical fingerprints and source assessment guiding air quality improvements by 2030 in Andalusia, southern Spain. Environ. Poll. 388, 127347. https://doi.org/10.1016/j.envpol.2025.127347.
Perrone, M.G., Larsen, B.R., Ferrero, L., Sangiorgi, G., De Gennaro, G., Udisti, R., Zangrando, R., Gambaro, A., Bolzacchini, E., 2012. Sources of high $PM_{2.5}$ concentrations in Milan, Northern Italy: molecular marker data and CMB modelling. Sci. Total Environ. 414, 343–355. https://doi.org/10.1016/j.scitotenv.2011.11.026.
Ponczek, M., Franco, M.A., Carbone, S., Rizzo, L.V., Monteiro dos Santos, D., Morais, F. G., Duarte, A., Barbosa, H., Artaxo, P., 2022. Linking the chemical composition and optical properties of biomass burning aerosols in Amazonia. Environ. Sci. Atmos 2, 252–269. https://doi.org/10.1039/D1EA00055A.
Rajesh, T.A., Ramachandran, S., 2020. Extensive and intensive properties of aerosol over distinct environments: influence of anthropogenic emissions and meteorology. J. Atmos. Solar–Terr. Phys. 202, 105223. https://doi.org/10.1016/j.jastp.2020.105223.
Romano, S., Perrone, M.R., Pavese, G., Esposito, F., Calvello, M.R., 2019. Optical properties of $PM_{2.5}$ particles: results from a monitoring campaign in southeastern Italy. Atmos. Environ. 203, 35–47. https://doi.org/10.1016/j.atmosenv.2019.01.037.
Rovira, J., Savadkoohi, M., Chen, G.I., Močnik, G., Aas, W., Alados-Arboledas, L., Artiñano, B., Aurela, M., Backman, J., Banerji, S., Beddow, D., Brem, B., Chazeau, B., Coen, M.C., Colombi, C., Conil, S., Costabile, F., Coz, E., de Brito, J.F., Eleftheriadis, K., Favez, O., Flentje, H., Freney, E., Gregorič, A., Gysel-Beer, M., Harrison, R., Hueglin, C., Hyvärinen, A., Ivančič, M., Kalogridis, A.-C., Keernik, H., Konstantinos, G., Laj, P., Liakakou, E., Lin, C., Listrani, S., Luoma, K., Maasikmets, M., Manninen, H.E., Marchand, N., dos Santos, S.M., Mbengue, S., Mihalopoulos, N., Nicolae, D., Niemi, J.V., Norman, M., Ovadnevaite, J., Petit, J.-E., Platt, S., Prévôt, A.S.H., Pujadas, M., Putaud, J.-P., Riffault, V., Rigler, M., Rinaldi, M., Schwarz, J., Silvergren, S., Teinemaa, E., Teinilä, K., Timonen, H., Titos, G., Tobler, A., Vasilescu, J., Vratolis, S., Yttri, K.-E., Yubero, E., Zíková, N., Alastuey, A., Petäjä, T., Querol, X., Yus-Díez, J., Pandolfi, M., 2025. A European aerosol phenomenology – 9: light absorption properties of carbonaceous aerosol particles across surface Europe. Environ. Inter. 195, 109185. https://doi.org/10.1016/j.envint.2024.109185.

Russell, P.B., Bergstorm, R.W., Shinozuka, Y., Clarke, A.D., De Carlo, P.F., Jiménez, J.L., Livingston, J.M., Redemann, J., Dubovik, O., Strawa, A., 2010. Absorption Ångström exponent in AERONET and related data as an indicator of aerosol composition. Atmos. Chem. Phys. 10, 1155–1169. https://doi.org/10.5194/acp-10-1155-2010.

Sandradewi, J., Prevot, A.S.H., Szidat, S., Perron, N., Alfarra, L.M., Lanz, V.A., Weingartner, E., Baltensperger, U., 2008. Using aerosol light absorption measurements for the quantitative determination of wood burning and traffic emission contributions to particulate matter. Environ. Sci. Technol. 42, 3316–3323. https://doi.org/10.1021/es702253m.

Savadkoohi, M., Pandolfi, M., Reche, M.C., Niemi, J.V., Mooibroek, D., Gloria Titos, G., Green, D.C., Tremper, A.H., Hueglin, C., Liakakou, E., Mihalopoulos, M., Stavroulas, I., Artiñano, B., Coz, E., Alados-Arboledas, L., Beddows, D., Riffault, V., De Brito, J.F., Bastian, S., Baudic, A., Costabile, F., Chazeau, B., Gómez-Amo, J.L., Estellés, V., Matos, V., van der Gaag, E., Gille, G., Luoma, K., Manninen, H.E., Norman, M., Silvergren, S., Petit, J.-E., Putaud, J.-P., Rattigan, O.V., Timonen, H., Tuch, T., Merkel, M., Weinhold, K., Vratolis, S., Vasilescu, J., Favez, O., Harrison, R. M., Lag, P., Wiedensohler, A., Hopke, P.H., Petäjä, T., Querol, X., 2023. The variability of mass concentrations and source apportionment analysis of equivalent black carbon across urban Europe. Environ. Inter. 178, 108081. https://doi.org/10.1016/j.envint.2023.108081.

Scerri, M., Kandler, K., Weinbruch, S., Yubero, E., Galindo, N., Prati, P., Caponi, L., Massabò, D., 2019. Estimation of the contributions of the sources driving $PM_{2.5}$ levels in a Central Mediterranean coastal town. Chemosphere 211, 465–481. https://doi.org/10.1016/j.chemosphere.2018.07.104.

Schmeisser, L., Andrews, E., Ogren, J.A., Sheridan, P., Jefferson, A., Sharma, S., Kim, J. E., Sherman, J.P., Sorribas, M., Kalapov, I., Arsov, T., Angelov, C., Mayol-Bracero, O. L., Labuschagne, C., Kim, S.-W., Hoffer, A., Lin, N.-H., Chia, H.-P., Bergin, M., Sun, J., Liu, P., Wu, H., 2017. Classifying aerosol type using in situ surface spectral aerosol optical properties. Atmos. Chem. Phys. 17, 12097–12120. https://doi.org/10.5194/acp-17-12097-2017, 2017.

Seinfeld, J.H., Pandis, S.N., 2016. Atmospheric Chemistry and Physics: from Air Pollution to Climate Change. John Wiley & Sons, Hoboken.

Suchánková, L., Mbengue, S., Zíková, N., Šmejkalová, A.H., Prokeš, R., Holoubek, I., Ždímal, V., 2024. A seven-year-based characterization of aerosol light scattering properties at a rural central European site. Atmos. Environ. 319, 120292. https://doi.org/10.1016/j.atmosenv.2023.120292.

Titos, G., Foyo-Moreno, I., Lyamani, H., Querol, X., Alastuey, A., Alados-Arboledas, L., 2012. Optical properties and chemical composition of aerosol particles at an urban location: an estimation of aerosol mass scattering and absorption efficiencies. J. Geophys. Res. 117, D04206. https://doi.org/10.1029/2011JD016671.

Tzanis, C., Varotsos, C., Christodoulakis, J., Tidblad, J., Ferm, M., Ionescu, A.R.-A., Lefevre, R.-A., Theodorakopoulou, K., Kreislova, K., 2011. On the corrosion and soiling effects on materials by air pollution in Athens, Greece. Atmos. Chem. Phys. 11, 12039–12048. https://doi.org/10.5194/acp-11-12039-2011.

Valentini, S., Bernardoni, V., Massabò, D., Prati, P., Valli, G., Vecchi, R., 2018. Tailored coefficients in the algorithm to assess reconstructed light extinction at urban sites: a comparison with the IMPROVE revised approach. Atmos. Environ. 172, 168–176. https://doi.org/10.1016/j.atmosenv.2017.10.038.

Varotsos, C., Ondov, J., Tzanis, C., Öztürk, F., Nelson, M., Ke, H., Christodoulakis, J., 2012. An observational study of the atmospheric ultra-fine particle dynamics. Atmos. Environ. 59, 312–319. https://doi.org/10.1016/j.atmosenv.2012.05.015.

Velazquez-García, A., Crumeyrolle, S., de Brito, J.F., Tison, E., Bourrianne, E., Chiapello, I., Riffault, V., 2023. Deriving composition-dependent aerosol absorption, scattering and extinction mass efficiencies from multi-annual high time resolution observations in Northern France. Atmos. Environ. 298, 119613. https://doi.org/10.1016/j.atmosenv.2023.119613.

Vörösmarty, M., Uzu, G., Jaffrezo, J.-L., Dominutti, P., Kertész, Z., Papp, E., Salma, I., 2023. Oxidative potential in rural, suburban and city centre atmospheric environments in central Europe. Atmos. Chem. Phys. 23, 14255–14269. https://doi.org/10.5194/acp-23-14255-2023.

Washenfelder, R.A., Attwood, A.R., Brock, C.A., Guo, H., Xu, L., Weber, L.J., Ng, N.L., Allen, H.M., Ayres, B.R., Baumann, K., Cohen, R.C., Draper, D.C., Duffey, K.C., Edgerton, E., Fry, J.L., Hu, W.W., Jiménez, J.L., Palm, B.B., Romer, P., Stone, E.A., Wooldridge, P.J., Brown, S.S., 2015. Biomass burning dominates brown carbon absorption in the rural southeastern United States. Geophys. Res. Lett. 42, 653–664. https://doi.org/10.1002/2014GL062444.

Zhang, Y., Albinet, A., Petit, J.E., Jacob, V., Chevrier, F., Gille, G., Pontet, S., Chrétien, E., Dominik-Sègue, M., Levigoureux, G., Močnik, G., Gros, V., Jaffrezo, J.-L., Favez, O., 2020. Substantial brown carbon emissions from winter residential wood burning over France. Sci. Total Environ. 743, 140752. https://doi.org/10.1016/j.scitotenv.2020.140752.